J Mol Model (2012) 18:3783–3792
DOI 10.1007/s00894-012-1387-2

ORIGINAL PAPER

Study on the enantioselectivity inhibition mechanism of acetyl-coenzyme A carboxylase toward haloxyfop by homology modeling and MM-PBSA analysis

Jin Tao · Guirong Zhang · Aijun Zhang · Liangyu Zheng · Shugui Cao

Received: 22 September 2011 / Accepted: 16 February 2012 / Published online: 7 March 2012
© Springer-Verlag 2012

Abstract Acetyl-coenzyme A carboxylase (ACCase) has been identified as one of the most important targets of herbicide Aryloxyphenoxypropionates (APPs). ACCase shows different enantioselectivity toward APPs, and only (*R*)-enantiomers of APPs have the herbicidal activity. In order to deeply understand the enantioselective recognition mechanism of ACCase, (*R*)-haloxyfop, which is a typical commercial herbicide from APPs, is selected and the relative binding free energy between ACCase and (*R*)-haloxyfop is investigated and compared with that between ACCase and (*S*)-haloxyfop by homology modeling and molecular mechanics-Poisson-Boltzmann surface area (MM-PBSA) method. Further free energy analysis reveals that the preference of ACCase toward (*R*)-haloxyfop is mainly driven by Van der Waals interaction. The analysis of the interaction between the active site residues of ACCase CT domain and (*R*)-haloxyfop shows the van der Waals interactions have a close relationship with the addition effect of each residue. An understanding of the enantioselective recognition mechanism between ACCase and haloxyfop is desirable to discover novel chiral herbicides.

Keywords Acetyl-coenzyme A carboxylase · Enantioselective recognition mechanism · Haloxyfop, Homology modeling · MM-PBSA analysis

J. Tao · A. Zhang · L. Zheng (✉) · S. Cao (✉)
Key Laboratory for Molecular Enzymology and Engineering of Ministry of Education, Jilin University, Changchun 130012, People's Republic of China
e-mail: lyzheng@jlu.edu.cn
e-mail: caosg@jlu.edu.cn

G. Zhang
College of Life Science, Jilin University, Changchun 130012, People's Republic of China

Introduction

Acetyl-coenzyme A carboxylase (ACCase; EC 6.4.1.2) is a key enzyme in fatty acid metabolism. It regulates fatty acid biosynthesis and oxidation, and catalyzes the ATP-dependent carboxylation of acetyl-CoA to produce malonyl-CoA [1–3]. The reaction is carried out in two steps, in which the first step is the ATP-dependent carboxylation of biotin catalyzed by biotin carboxylase, and the second step consists of the transfer of the carboxyl group from biotin to acetyl-CoA catalyzed by carboxyltransferase (CT) [4].

Two isoforms of ACCase have been identified in plant cells [5, 6]. Heteromeric ACCase, locating at chloroplast in most plants, is composed of four subunits, biotin carboxyl carrier protein (BCCP), biotin carboxylase (BC), carboxyltransferases α and β (CT-α and CT-β). Homomeric ACCase, locating at cytosol, is composed of a single strand peptide including four function domains, BC, BCCP, CT-α and CT-β. However, there is an exceptional case in *Poaceae* grasses, the ACCase in plastid is homomeric which is encoded by a nuclear gene distinct from that coding for the cytosolic ACCase isoform [7].

The chloroplastic, multidomain form of ACCase has been identified as the target of two classes of herbicides: aryloxyphenoxypropionates (APPs) and cyclohexanediones (CHDs) [8–10]. Both kinds of herbicides selectively inhibit the carboxyltransferase (CT) activity of ACCase and block the growth of *Poaceae* grasses [11, 12]. Research works have shown ACCase is significantly more sensitive to (*R*)-APPs [13, 14]. However, the enantioselective recognition mechanism surrounding the binding of (*R*, *S*)-APPs to ACCase is not clear. The major obstacle is lack of the corresponding three-dimension structures of the CT domain of ACCase from *Poaceae* and the complex binding modes between CT and (*R*)- or (*S*)-APPs.

Recently, the crystal structures of the ACCase CT domain (PDB entry: 1OD2 and 1OD4) of *Sacharomyces cerevisiae* and its complex with APPs (PDB entry: 1UYR and 1UYS) were successfully determined at 2.7 and 2.5 Å resolution, respectively [8, 15]. It gave a direct guiding on how (*R*)-APPs interacted with the CT domain of ACCase on atom level. Although the CT domain of ACCase from the yeast was so different from that of *Poaceae*, for instance the CT domain from yeast was insensitive to APPs, the CT domains from yeast and Poaceae were both multidomain proteins and had a high sequence similarity. Using ACCase CT three-dimensional structure from *S. cerevisiae* as template, the ACCase CT domain from *Poaceae* was constructed successfully by homology modeling, and the interactions between the CT domain and APPs were analyzed by molecular dynamic simulations and molecular mechanics-Poisson-Boltzmann surface area (MM-PBSA) calculations [16–19]. However, the above interaction studies were mainly focused on the resistant mechanism of ACCase, and little attention was paid to the enantioselective recognition mechanism of ACCase toward APPs.

In this article, we use homology modeling to establish the theoretical models of the three-dimensional dimer structure of CT from *Alopecurus myosuroides*, and its complexes with (*R*)- and (*S*)-haloxyfop from APPs (Scheme 1). The interactions between CT and haloxyfop are investigated. Moreover, the relative binding free energy difference between CT domain and (*R*)- or (*S*)-haloxyfop is reproduced and analyzed by MM-PBSA method.

Materials and methods

Materials

The *A. myosuroides* ACCase CT domain sequence (entry: Q8LRK2) was obtained from TrEMBL database. The crystal structures of the free CT from *S. cerevisiae* (entry: 1OD2) and (*R*)-haloxyfop-CT complexes (entry: 1UYS) were obtained from PDB database.

Homology modeling

The CT dimer from *S. cerevisiae* was formed by the side-to-side arrangement of the two monomers including N-subdomain and C-subdomain, namely, the N-subdomain of one monomer was placed next to the C-subdomain of the other. Two identical active sites were located in the interface between N-subdomain of one monomer and C-subdomain of the other [8, 10, 15]. As the molecular dynamics simulation for this large size scale on nanosecond timescale was too time-consuming, herein only one of the active sites was considered and a truncated form of CT dimer was made as the template. The truncated dimer consisted of N-subdomain of one monomer from residue 1575–1767 and a C-subdomain of another monomer from 1886–2097, each of which contained the critical β-β-α core region. The two monomeric chains were superimposed onto the crystal structure of the CT domain from yeast (1OD2), keeping the same relative orientation of the two subunits.

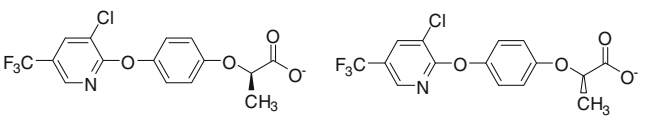

Scheme 1 Chemical structures of (*R*)-halxoyfop (left) and (*S*)-haloxyfop (right)

Based on the template, the truncated dimer of the free CT from *A. myosuroides* was modeled with MODELLER 9v1 program [20–22]. The sequence alignments of N-subdomain and C-subdomian between *S. cerevisiae* and *A. myosuroides* were extracted from the Pfam database (entry: PF01039). To ensure accurate alignments for homology modeling, the alignments were also redone and manually inspected using CLUSTALX 1.83 program.

However, for the modeling of the complex structure of CT domain from *A. myosuroides* with (*R*)-haloxyfop, the double templates were needed, just because the complex structure of CT dimer of yeast with (*R*)-haloxyfop (PDB code: 1UYS) missed the residues in 2048–2080 and 1959–1964, and the free CT structure (PDB code: 1OD2) was used as a complementary template for these missing residues.

For both free CT from *A. myosuroides* and the complex of CT and (*R*)-haloxyfop, the number of homology modeling structures was set to 100, and the other parameters were default. The modeled truncated CT dimer contained a total of 400 residues, which were renumbered as following: the C-subdomain of one monomer was renumbered from 1 to 211, and the N-subdomain of the other monomer was renumbered from 212 to 400. The quality of modeling was evaluated by the energy function score in Modeller and a series of other tools, such as PROCHECK [23], WHAT-IF [24] and VERIFY3D [25]. The best model was picked for the following MD calculations.

Based on the best modeled complex of CT dimer from *A. myosuroides* with (*R*)-haloxyfop, the complex structure of CT-(*S*)-haloxyfop was easily constructed by inverting the methyl group and the hydrogen on the chiral carbon atom of (*R*)-haloxyfop with Insight II package (Accelrys) on SGI fuel station (Silicon Graphics, Inc.), and then subjected to energy minimization until the energy was converged to 0.1 kcal mol^{-1} $Å^{-1}$ with CVFF force field [26].

Molecular dynamics

Five systems, (*R*)- and (*S*)-haloxyfop-CT complexes, (*R*)- and (*S*)-haloxyfop extracted from the complexes and free CT, were

subjected to molecular dynamic simulation with Amber 9 [27] on a cluster with 24 intel Xeron 2 CPU (2.0 GHz). The Duan force field [28, 29] and GAFF force field [30] were adopted for CT and haloxyfop, respectively. Charges of haloxyfop were derived by AM1-BCC method [31, 32].

Before the formal molecular dynamic simulations were carried out, the following elaborated preparing protocols were adopted. For (*R*)- and (*S*)-haloxyfop-CT complexes, the systems were firstly automatically added hydrogen and then subjected to energy minimization with generalized Born implicit water model [33–35] with decreasing force constrained on non-hydorgen atom until the system converged. Secondly, both systems were neutralized by adding Na^+ and then solvated in an octahedral box of TIP3P water molecules [36], which extended at 15 Å from any given atom in the systems. The water enclosed systems were repeatedly minimized for 2000 steps SD and 2000 steps CG with decreasing force on protein, and followed by a minimization with system free. Thirdly, the systems were slowly heated from 0 to 300 K with decreasing force on protein over the 200 ps. The (*R*)- and (*S*)-haloxyfop system followed a similar preparing procedure without minimization in GB implicit solvent model for simplicity.

After the preparing procedures finished, the formal molecular dynamics were run for 10.2 ns for free CT dimer, (*R*)- and (*S*)-haloxyfop-CT complex, and 2 ns for the (*R*)- and (*S*)- haloxyfop, respectively. During the simulation, the particle mesh Ewald method [37] was selected for periodic long range electrostatic force and a 10 Å cutoff for nonbonding Van der Waals interactions. All bonds involving hydrogen atoms were constrained using the SHAKE algorithm [38]. Constant temperature 300 K was maintained using Langevin thermostats with the collision frequency of 1.0 [39, 40] and constant pressure 1 atm was controlled by isotropic position scaling with the pressure relaxation time of 2.0 ps [41]. A time step of 2 fs was used to integrate the equations of motion. The coordinates were saved every 20 ps during the entire of simulation process.

Binding free-energy calculation

The binding free energies were calculated by using the molecular mechanics-Poisson-Boltzmann surface area (MM-PBSA) method [42] with mm pbsa procedure in Amber 9. In this method, the binding free energy, ΔG_{bind} could be evaluated as a sum of the changes in the MM gas-phase energy (ΔE_{MM}), solvation free energy (ΔG_{solv}) and entropy contribution ($-T\Delta S$) as follows.

$$\Delta G_{bind} = \Delta E_{MM} + \Delta G_{solv} - T\Delta S \quad (1)$$

$$\Delta E_{MM} = \Delta E_{cou} + \Delta E_{vdw} \quad (2)$$

$$\Delta G_{solv} = \Delta G_{pb} + \Delta G_{np} \quad (3)$$

$$\Delta G_{np} = \gamma SASA + \beta \quad (4)$$

$$\Delta G_{ele} = \Delta E_{cou} + \Delta G_{pb} \quad (5)$$

Herein, the entropy contribution to the structure-similar inhibitors was almost same and was neglected since our aim was to calculate the relative binding free energy difference [43]. The MM gas-phase energy, including Coulomb interaction (ΔE_{cou}) and Van der Waals interaction (ΔE_{vdw}) was directly calculated with force field. Electrostatic solvation free energy (ΔG_{pb}) was calculated by the numerical finite-difference solution to the PB equation. The dielectric constants used are 1 for the solute and 80 for the solvent water. Both electrostatic solvation free energy (ΔG_{pb}) and Coulomb interaction (ΔE_{cou}) belong to the electrostatic contribution (ΔG_{ele}). The solvent-accessible-surface area (SASA) was estimated using standard procedure by setting option NPOPT and RADIOPT to 1 and 0. The nonpolar solvation energy (ΔG_{np}) was successively calculated using Eq. 4 with parameters γ=0.00542 kcal mol^{-1} and β=0.92 kcal mol^{-1}, which were widely used in many MM-PBSA free energy calculations [16–19].

To further anatomize the binding free energy between the ligand and protein, the binding free energy was dissected into two sections [44], including the intramolecular interactions caused by the transformation from the unbound to bound conformation and the intermolecular interactions of the ligand and protein in their bound conformation.

There are two protocols to calculate the MM/PBSA binding free energy: (1) by one trajectory (complex) and (2) by three trajectories (free ligand, free protein and complex). The protocol using one trajectory assumed that the protein didn't have conformation changes during the binding with ligand. However, the protocol using three trajectories needed to consider the conformation change of the protein during the binding, and the calculated energy was thus much closer to the real binding free energy. Herein, the protocol based on one trajectory was used to calculate the intermolecular binding free energy, to which each contribution was indicated with a superscript "int", such as ΔE_{cou}^{int}, ΔE_{vdw}^{int}, ΔG_{np}^{int}, ΔG_{pb}^{int}, ΔG_{ele}^{int} and ΔG_{bind}^{int}. The protocol based on three trajectories were used to calculate the binding free energy (ΔG_{bind}) and the binding free energy difference between (*R*)- and (*S*)-haloxfop. Regarding the intramolecular binding free energy contributed by both of the haloxfop and CT protein, it would be calculated using the bound conformations (complex trajectory) and the unbound conformations (free protein and ligand trajectory). Similarly, these contributions were indicated with superscript "tra", such as ΔG_{lig}^{tra} (ligand intramolecular

binding free energy), ΔG_{pro}^{tra} (protein intramolecular binding free energy), ΔG_{bind}^{tra} (intramolecular binding free energy). Three hundred structures were sampled from the MD trajectory from 4.2 ns to 10.2 ns for free CT dimmer, (*R*)- and (*S*)-haloxyfop-CT complex with 20 ps interval. The final averages of the binding free energy over these samples were taken to compute the association difference between (*R*)- and (*S*)-haloxfop-CT complex. In the same way, 100 structures were sampled from the MD trajectory of (*R*)- and (*S*)-haloxyfop with 20 ps interval in order to calculate the transformation energy difference of the ligand from water to enzyme.

In addition, Insight II package (Accelrys) was used to analyze the Van der Waals interactions between haloxyfop and each residue in the active site of CT with CVFF force field.

Results and discussion

Homology modeling

Different from the previous report that only one active site of the complete CT dimer was subjected to do the molecular dynamic simulations [18, 19], herein we took a different way that a truncated but structurally independent dimer was constructed and used in molecular dynamic simulation. Our conception was originated from the bacterial CT active form, which was constituted of CT-α and CT-β subunits corresponding to C-subdomain and N-subdomain from eukaryotic CT. Furthermore, the structural analysis of *S. cerevisiae* also showed the C-subdomain and N-subdomain of one monomer were structurally independent and had little interaction with N-subdomain or C-subdomain from the same monomer [8], implicating that the truncated dimer protocol practicable. Our truncated CT dimer consisted of N-subdomain of one monomer (residues 212 to 400, corresponding to residues 1575–1767 of *S. cerevisiae*) and a C-subdomain of the other monomer (residues 1 to 211, corresponding to residues 1886–2097 of *S. cerevisiae*). Each contained the complete critical β-β-α core and insertion region, which kept the proper topology and dimerization. The molecular dynamic simulations also showed that the core structure and the active site of CT were not significantly changed compared with that in previous reports [18, 19]. Obviously, our truncated CT dimer molecular simulation was much more time-efficient, and it provided an alternative protocol to analyze the molecular interactions between CT and its ligand using molecular dynamic simulation.

High homology identity was critical for accurate homology modeling. The total sequence identity of the truncated CT dimer between *S. cerevisiae* and *A. myosuroides* was 52.3%, where the N-subdomain identity was 53.4% and C-subdomain identity was 51.4% (Fig. 1). It enabled us to accurately construct the *A. myosuroides* CT dimer.

The free CT dimer and (*R*)-haloxyfop-CT complex model, which had the lowest energy score, were selected from the 100 models based on the energy function in Modeller and a series of structure-examination software for evaluation. In Ramachandran plot (Fig. 2 a and b), the 90.1% and 90.4% of residues without glycine and proline of the CT dimer, were located respectively in the most favored regions for free CT dimer and (*R*)-haloxyfop-CT complex, consistent with the expectation of over 90% in the most favored regions. Only one residue (0.3%), Ile 377, was in the disallowed regions. Notably, the corresponding residue, Gln 1744, in *S. cerevisiae* CT domain was also in the disallowed regions (Fig. 2 c). The WHAT-IF packing scores between the truncated template and the built models were similar and the scores for most residues were above −5.0 (Fig. 3), indicating our structure were reasonable. A similar trend was observed by VERIFY-3D evaluation (Fig. 4), and the score profiles were similar for the templates and the built models. All these suggested that the modeled structures of the free CT and (*R*)-haloxyfop-CT complex were reasonable.

Molecular dynamics

Five systems, (*R*)- and (*S*)-haloxyfop-CT complexes, (*R*)- and (*S*)-haloxyfop extracted from the complexes and free CT were subjected to molecular dynamic simulations. For all three system, (*R*)- and (*S*)-haloxyfop-CT complexes and free CT, the plot of root mean square deviation (RMSD) values from the starting structure of all the alpha carbon of CT dimer increased and fluctuated greatly but different each other (Fig. 5 black lines).

However, after removing the residues 162–194 (corresponding to α6B-α6C-α6D of *S. cerevisiae* CT domain), part of the insertion region of C-subdomain, the plots of RMSD values were quickly equilibrated and harmonically fluctuated around a platform of 2 Å for all three systems (Fig. 5 red lines), which was similar to previous reports [18, 19]. The RMSD values also showed that the structure without α6B-α6C-α6D was not significantly changed from the starting structure during the molecular dynamic simulation, and confirmed that our truncated CT dimer was structure-independent. Obviously, the RMSD values for all alpha carbons were the results of rigid body motion of the residues 162–194. This fact was consistent with the phenomena that the corresponding residues 2048–2080 were always unresolved in the crystal structure of *S. cerevisiae* CT. This region was also observed to be far away from the active site and isolated by the surrounded water, implying this region had little effect on haloxyfop binding and the enatioselectivity of CT.

To analyze the interaction between (*R*)- or (*S*)-haloxyfop and CT, an average structure was extracted from 8.2 ns to 10.2 ns for both (*R*)-haloxyfop-CT and (*S*)-haloxyfop-CT

```
Yeast_N   1575         EYPRGRQFVVVANDITFKIGSFGPQEDEFFNKVTEYARKRGIPRIYLAANSGARIGMAEE
Alope_N   1655 (212)  EFPSGRQIIVIANDITFRAGSFGPREDAFFEAVTNLACEKKLPLIYLAANSGARIGIADE
                      *:* ***::*:******: *****:** **: **: * :: :* ************:*:*

Yeast_N   1635         IVPLFQVAWNDAANPDKGFQYLYLTSEGMETLKKFDKENSVLTERTVINGEERFVIKTII
Alope_N   1715 (272)  VKSCFRVGWTDDSSPERGFRYIYMTDEDHDRIGS----SVIAHKMQLDSGEIRWVIDSVV
                      : . *:*.*.* :.*::**:*:*:*.*. : : .    . :  :  : .** *:**.:::

Yeast_N   1695         GSEDGLGVECLRGSGLIAGATSRAYHDIFTITLVTCRSVGIGAYLVRLGQRAIQVEGQPI
Alope_N   1771 (328)  GKEDGLGVENIHGSAAIASAYSRAYEETFTLTFVTGRTVGIGAYLARLGIRCIQRIDQPI
                      *.******* ::**.  **.* ****.: **:*:** *:*******.*** *.**  .***

Yeast_N   1755         ILTGAPAINKMLG  1767
Alope_N   1831 (388)  ILTGFSALNKLLG  1843 (400)
                      **** .*:**:**

Yeast_C   1886       GIPLGVIGVETRTVENLIPADPANPNSAETLIQEPGQVWHPNSAFKTAQAINDFNNGEQL
Alope_C   1961 (1)   GIPVGVIAVETQTMMQLVPADPGQPDSHERSVPRAGQVWFPDSATKTAQAMLDFNR-EGL
                     ***:***.***:*: :*:****.:*:* *  : ..****.*:** *****: ***.  * *

Yeast_C   1946        PMMILANWRGFSGGQRDMFNEVLKYGSFIVDALVDYKQPIIIYIPPTGELRGGSWVVVDP
Alope_C   2020 (60)   PLFILANWRGFSGGQRDLFEGILQAGSTIVENLRTYNQPAFVYIPKAAELRGGAWVVIDS
                      *::***************:*: :*: ** **: *  *:** ::*** :.*****:***:*.

Yeast_C   2006         TINADQMEMYADVNARAGVLEPQGMVGIKFRREKLLDTMNRLDDKYRELRSQLSNKSLAP
Alope_C   2080 (120)  KINPDRIECYAERTAKGNVLEPQGLIEIKFRSEELKECMGRLDPELIDLKARLQGANGSL
                       .**.*::* **: .*:..******:: **** *:* : *.*** :  :*:::*.. . :

Yeast_C   2066         EVHQQISKQLADRERELLPIYGQISLQFADLH  2097
Alope_C   2140 (180)  SDGESLQKSIEARKKQLLPLYTQIAVRFAELH  2171 (211)

                      .  :.:.*.:  *:::***:* **:::**:**
```

Fig. 1 The alignment of CT domain from *S. cerevisiae* and *A. myosuroides*. Yeast_N and Yeast_C represent the N-subdomain and C-subdomain of *S. cerevisiae* CT domain, respectively. Alope_N and Alope_C represent the N-subdomain and C-subdomain of *A. myosuroides* CT domain, respectively. The numbers in the bracket are the renamed residue sequence of *A. myosuroides* CT domain. The asterisk symbol (*) indicates a residue that is identical between *S. cerevisiae* and *A. myosuroides*. A colon symbol (:) indicates a residue that is very similar between *S. cerevisiae* and *A. myosuroides*. A dot symbol (.) indicates a residue that is less similar between *S. cerevisiae* and *A. myosuroides*

complex, respectively (Fig. 6). For both (*R*)- and (*S*)-haloxyfop, it was found that the pyridyl ring was π-π stacked with Phe 70 and Tyr 371 of CT domain like a sandwich and the phenyl ring Van der Waals interacted with Gly 111, Gly 112, Gly 367 and Ile 368 of CT domain. In addition, two hydrogen bonds were formed between one of the carboxyl oxygen of (*R*)- or (*S*)-haloxyfop and the main-chain amides of Ala 264 and Ile 368 of CT domain (Fig. 6 yellow dot line). The binding modes were similar with that described in Tong's work [10], where the corresponding residues were Phe 1956' (primed residue number indicates the CT domain of the other monomer), Tyr 1738, Ala 1627, Gly 1997', Gly 1998', Gly 1734 and Ile 1735. However, some residues locating in CT active site were different between *S. cerevisiae* and *A. myosuroides*, although the CT active site was much conserved. The renumbered residues 207 and 338 in modeled *A. myosuroides* CT domain were glycine and isoleucine, where the corresponding residues in whole ACCase sequence of *A. myosuroides* were residue 2096 and 1781, whereas in *S. cerevisiae* were alanine (residue 2022) and leucine (residue 1705). The experiments by other group had confirmed that ACCase from *A. myosuroides* with single mutation G2096A and I1781L was (R)-haloxyfop-resistant [13, 17], which explained why the the *S. cerevisiae* has lower affinity and enantioselectivity toward (R)-haloxyfop than that of *A. myosuroides*. Our previous computational study also showed that

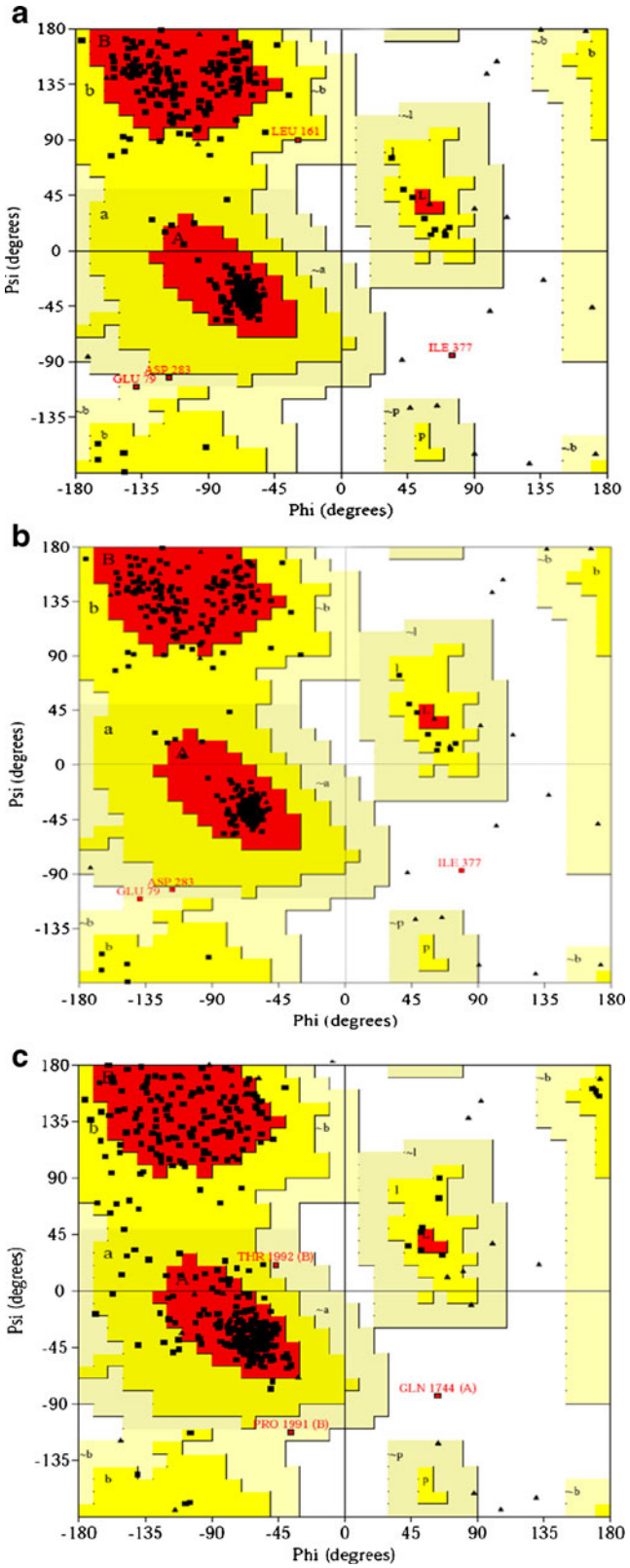

Fig. 2 The Ramachandran plots for the free CT of *A. myosuroides* (**a**), (*R*)-haloxyfop-CT complex (**b**) and the template CT of *S. cerevisiae* (**c**)

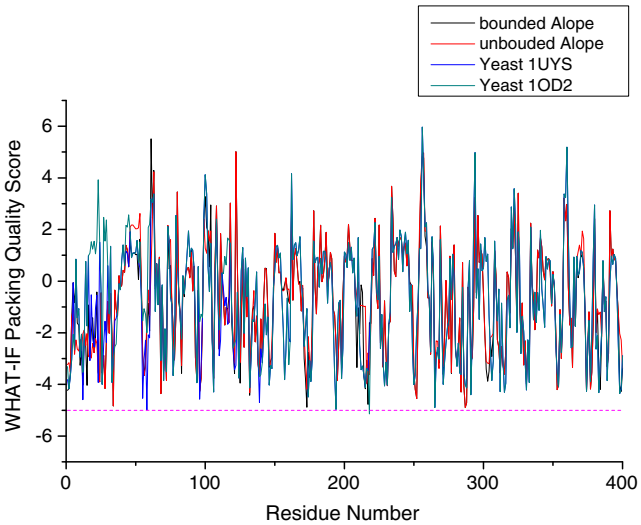

Fig. 3 WHAT-IF packing quality score profiles calculated for the template and homology models. The dash line is the line with score of −5. The residues with score lower than this value may be unreasonable. "Alope" is the abbreviation of "*Alopecurus myosuroides*"

I1781L mutation of *poaceae* grass could produce the steric hindrance between the side chain of mutated residue leucine and the chiral methyl group of haloxyfop [16]. G2096A mutation was the substitution of the small group with large one and was argued to have effects on the conformation change of binding pocket [19].

Binding free energy calculation

Many contributions could affect the affinity or enantioselectivity between ligand and protein, such as electrostatic interaction, Van der Waals hydrophobic interaction, hydrogen bonding interaction and so on.

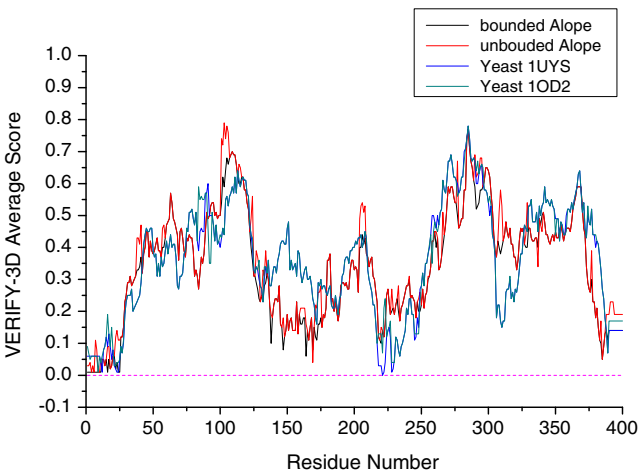

Fig. 4 VERIFY-3D score profiles calculated for the template and the homology models. The dash line is the line with score of 0. The residues with score lower than this value may be unreasonable. "Alope" is the abbreviation of "*Alopecurus myosuroides*"

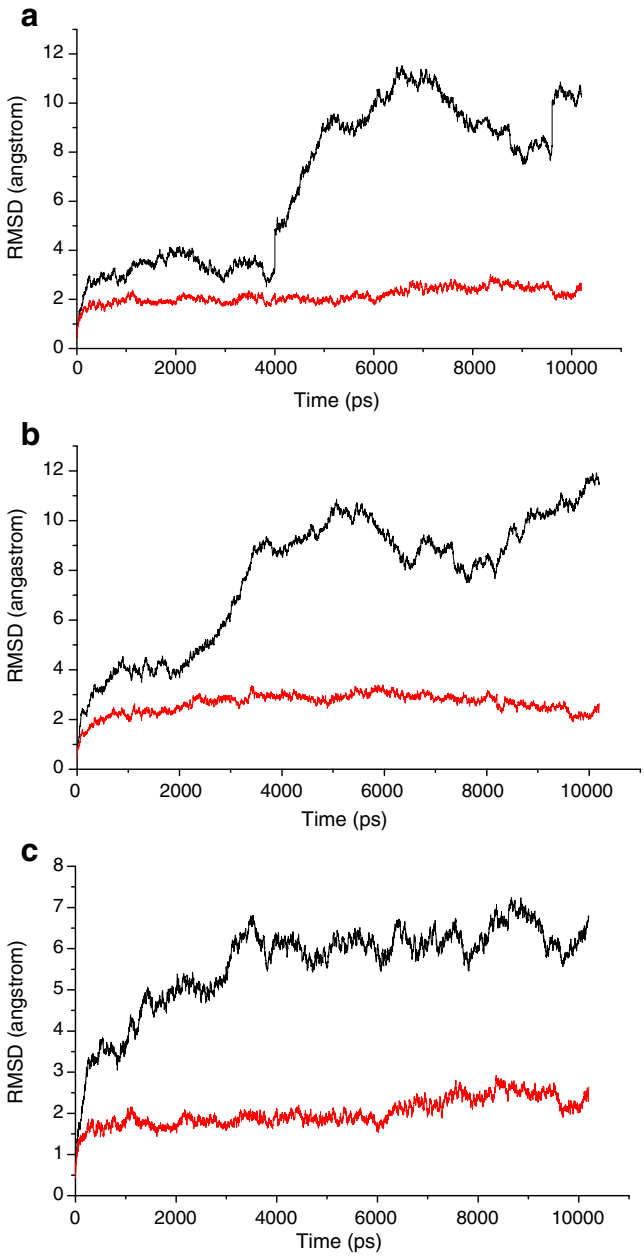

Fig. 5 Root mean square derivation (RMSD) of the truncated CT domain dimer (alpha carbon) in free CT (**a**), (*R*)-haloxyfop-CT complex (**b**) and (*S*)-haloxyfop-CT complex (**c**) to the starting structure. The black line is calculated for the whole CT dimer. The red line is calculated for the CT dimer without α6B-α6C-α6D

In order to find what were the major factors for the enantioselective recognization of CT domain, the binding free energies of (*R*)- and (*S*)-haloxyfop and various contributions to the binding were calculated using MM-PBSA method (Table 1). The calculated binding free energy difference ($\Delta\Delta G_{bind}$) between the enantiomers was −2.80 kcal mol^{-1}, which consistent with the experimental value in literature, −3.10 kcal mol^{-1} [45]. The free energy analysis showed that the Van der Waals interaction (ΔE_{vdw}^{int}) was the major drive to the association for both (*R*)- and (*S*)-haloxyfop, −48.07 kcal mol^{-1} and −45.86 kcal mol^{-1}, respectively. Also, the Van der Waals interaction played a major role on the enantioselective recognition of CT toward haloxyfop, since the difference between (*R*)-haloxyfop and (*S*)-haloxyfop was −2.21 kcal mol^{-1}, which was the largest contribution to the binding free energy difference. Nonpolar solvation free energy (ΔG_{np}^{int}) contributed less to the association and the values for (*R*)-haloxyfop and (*S*)-haloxyfop were similar, −5.18 kcal mol^{-1} and −5.15 kcal mol^{-1} respectively. Its contribution to the enantioselectivity of CT could be neglected. The electrostatic energy (ΔG_{ele}^{int}) which consisted of polar solvation free energy (ΔG_{pb}^{int}) and Coulomb interaction (ΔE_{cou}^{int}) was unfavorable for both (*R*)-haloxyfop and (*S*)-haloxyfop binding, 12.46 kcal mol^{-1} and 12.43 kcal mol^{-1} respectively. Although the polar solvent energy and the Coulomb interaction had a large effect on the energy difference between the enantiomers, their contributions were compensable to each other. So the electrostatic interaction had almost no effect on the enantioselectivity of CT.

Besides the above intermolecular interaction contribution, the CT dimmer also went through a conformational transformation during the binding with haloxyfop [15]. Herein, the free energy change (ΔG_{bind}^{tra}) of the system between the bound state and unbound state, which arose from the intramolecular interaction, was also calculated (Table 1). It consisted of ligand intramolecular binding free energy (ΔG_{lig}^{tra}) and protein intramolecular binding free energy (ΔG_{pro}^{tra}). All the intramolecular binding free energies were positive, which suggested that the conformation changes needed energy. It was also observed that these energies were not very large and the largest one was only 3.66 kcal mol^{-1}, which implied that the CT conformation changes could readily happen. In addition, the absolute values of intramolecular binding free energy of CT (3.28 kcal mol^{-1} and 3.66 kcal mol^{-1}) were much higher than those of the ligand (0.51 kcal mol^{-1} and 0.72 kcal mol^{-1}), which was consistent with our common knowledge. The conformation change was more favorable for (*R*)-haloxfop-CT system (3.79 kcal mol^{-1}) than (*S*)-haloxfop-CT system (4.38 kcal mol^{-1}).

All in all, MM-PBSA free energy analysis showed that the enantioselective recognization of CT to haloxyfop was mainly determined by the van der Waals interaction difference between (*R*)- haloxyfop and (*S*)-haloxyfop binding to the hydrophobic cavity of CT dimer.

Since the Van der Waals interactions difference was the major reason for the enantioselectivity of CT, further Van der Waals interactions between the active site residues of CT and (*R*)- or (*S*)-haloxyfop were investigated (Fig. 7). It was clearly shown that the total Van der Waals interaction difference was well-proportioned distributed around residues in CT which directly interacted with haloxyfop. No single residue majorly contributed

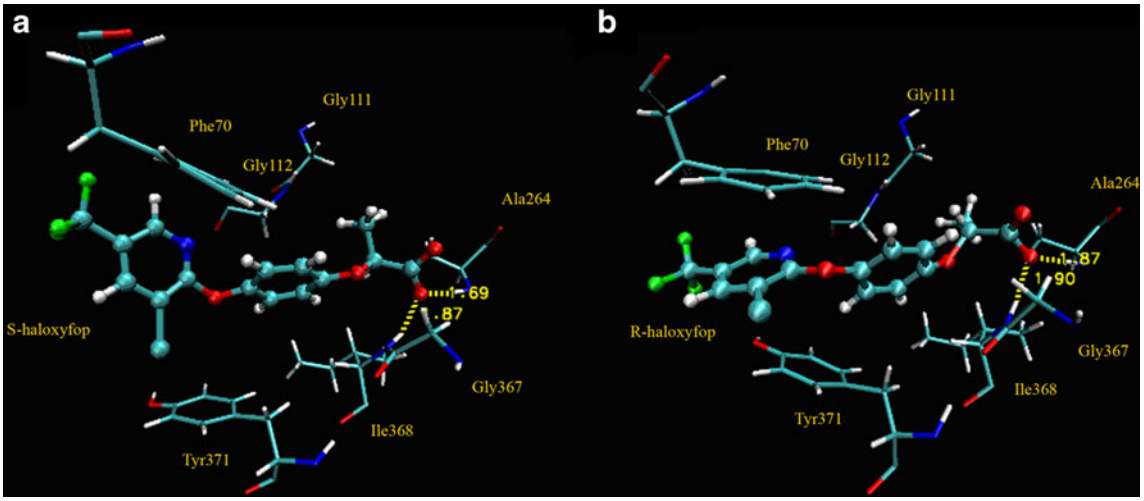

Fig. 6 The binding mode of (*S*)-haloxyfop-CT (A) and (*R*)-haloxyfop-CT (B). Haloxyfop is presented with ball and stick y model and the residues of CT are presented with sticks coloring according to their atom type. The hydrogen bonds are labeled with yellow dot line

to the total energy difference as a hot spot. The total Van der Waals interactions difference was the results of a sum of each residue. It also suggested that the active site was tightly fit with (*R*)-haloxyfop, which was consistent with the previous report [46].

Table 1 The various binding free energies for (*R*) and (*S*)-haloxyfop[a]

		(*R*)-	(*S*)-	Delta[b]	
		calc	calc	calc	exp[c]
Inter	ΔE_{cou}^{int}	11.31±6.23	5.33±7.85	5.98	
	ΔE_{vdw}^{int}	−48.07±3.74	−45.86±3.16	−2.21	
	ΔG_{np}^{int}	−5.18±0.65	−5.15±0.43	−0.03	
	ΔG_{pb}^{int}	1.15±7.12	7.10±7.23	−5.95	
	ΔG_{ele}^{int}	12.46±6.91	12.43±7.72	0.03	
	ΔG_{bind}^{int}	−40.79±7.39	−38.58±8.07	−2.21	
Intra	ΔG_{lig}^{tra}	0.51	0.72	−0.21	
	ΔG_{pro}^{tra}	3.28±4.51	3.66±4.19	−0.38	
	ΔG_{bind}^{tra}	3.79	4.38	−0.59	
Total	ΔG_{bind}	−37.00	−34.20	−2.80	−3.10

[a] All values in the table are given in kcal mol^{-1}. The intermolecular free energy components (ΔE_{cou}^{int}, ΔE_{vdw}^{int}, ΔG_{np}^{int}, ΔG_{pb}^{int}, ΔG_{ele}^{int}, ΔG_{bind}^{int}) in Table 1 have standard derivation since the protein-ligand complex, protein and ligand have the same number of frames (300). It is the same for ΔG_{pro}^{tra} since the bounded protein and unbounded protein both have the same number of frames (300). For ΔG_{lig}^{tra}, ΔG_{bind}^{tra} and ΔG_{bind}, only the average value is obtained since the ligand of unbounded state has a different number of frames (100)

[b] Component(R)-Component(S)

[c] Value is deduced from equation $\Delta\Delta G_{tot} = -RT\ln(K_i^R/K_i^S)$, in which $K_i^R/K_i^S < 1/200$

Conclusions

The three-dimensional structures of the free CT from *A. myosuroides*, (*R*)- and (*S*)-haloxyfop-CT complex were constructed by homology modeling, whose reliability were confirmed using PROCHECK, WHAT-IF and VERIFY3D. Homology modeling and MM-PBSA analysis revealed that the herbicide (*R*)-haloxyfop had more inhibiting activity than that of (*S*)-haloxyfop, which was mainly determined by the difference of Van der Waals interactions between (*R*)- and (*S*)-haloxyfop binding to CT dimer. These findings would help to clarify the molecular mechanism of stereochemistry-activity relationships between the inhibitors and CT domain of ACCase from *Poaceae*, and establish a basis for the discovery of more potent chiral inhibitors of ACCase.

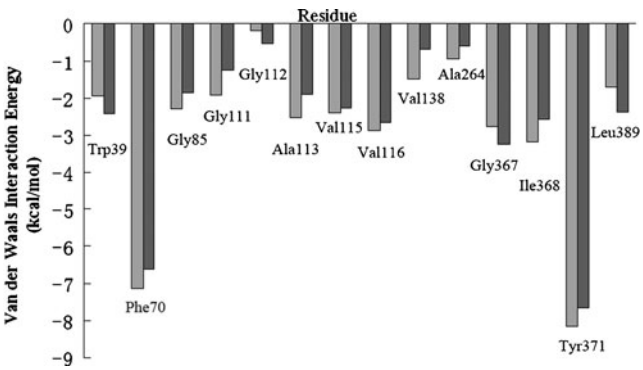

Fig. 7 Van der Waals interactions between the active site residues of CT and (*R*)- or (*S*)-haloxyfop. The interaction for (*R*)-haloxyfop is in black and the grey for (*S*)-haloxyfop

Acknowledgments The authors are grateful for the financial support from National Natural Science Foundation of China (no. 20802025, 30870539, 20432010 and 20672045), Jilin Provincial Science &Technology Sustentation Program (no.20110436), Basic operating expenses of Jilin University and 985 Project of Jilin University. The authors acknowledge Professor Yan Feng for the usage of soft Amber 9.

References

1. Wakil SJ, Stoops JK, Joshi VC (1983) Fatty acid synthesis and its regulation. Ann Rev Biochem 52:537–579
2. Harwood JL (1988) Fatty acid metabolism. Ann Rev Plant Physiol 39:101–138
3. Nikolau BJ, Ohlrogge JB, Wurtele ES (2003) Plant biotin-containing carboxylases. Arch Biochem Biophys 414:211–222
4. Davis MS, Solbiati J, Cronan JE Jr (2000) Overproduction of acetyl-CoA carboxylase activity increases the rate of fatty acid biosynthesis in Escherichia coli. J Biol Chem 275:28593–28598
5. Sasaki Y, Konishi T, Nagano Y (1985) The compartmentation of acetylcoenzyme A carboxylase in plants. Plant Physiol 108:445–449
6. Post-Beittenmiller D (1996) Biochemistry and molecular biology of wax production in plants. Plant Mol Biol 47:405–430
7. Konishi T, Shinohara K, Yamada K, Sasaki Y (1996) Acetyl-CoA carboxylase in higher plants: Most plants other than gramineae have both the prokaryotic and the eukaryotic forms of this enzyme. Plant Cell Physiol 37:117–122
8. Zhang H, Yang Z, Shen Y, Tong L (2003) Crystal structure of the carboxyltransferase domain of acetyl-coenzyme A carboxylase. Science 299:2064–2067
9. Sasaki Y, Nagano Y (2004) Plant acetyl CoA carboxylase structure, biosynthesis, regulation, and gene mainpulation for plant breeding. Biosci Biotechnol Biochem 68:1175–1184
10. Tong L (2005) Acetyl-coenzyme A carboxylase: crucial metabolic enzyme and attractive targer for drug discovery. Cell Mol Life Sci 62:1784–1803
11. Konishi T, Sasaki Y (1994) Compartmentalization of two forms of acetyl-CoA carboxylase in plants and the origin of their tolerance toward herbicides. Proc Natl Acad Sci 91:3598–3601
12. Devine MD, Shukla A (2000) Altered target sites as a mechanism of herbicide resistance. Crop Prot 19:881–889
13. Rendina AR, Craig-Kennard AC, Beaudoi JDK, Breen M (1990) Inhibition of acetyl-coenzyme A carboxylase by two classes of grassselective herbicides. J Agric Food Chem 38:1282–1287
14. Alban C, Baldet P, Douce R (1994) Localization and characterization of two structurally different forms of acetyl-CoA carboxylase in young pea leaves, of which one is sensitive to aryloxyphenoxypropionate herbicides. Biochem J 300:557–565
15. Zhang H, Tweet B, Tong L (2004) Molecular basis for the inhibition of the carboxyltransferase domain of acetyl-coenzyme-A carboxylase by haloxyfop and diclofop. Proc Natl Acad Sci 101:5910–5915
16. Tao J, Zhao B, Tian XM, Zheng LY, Cao SG (2010) Analysis of a critical residue determining herbicide efficiency sensitivity in carboxyltransferase domain of acetyl-CoA carboxylase from poaceae by homology modeling and free energy simulation. Chem Res Chin Univ 26:816–821
17. Zhu XL, Zhang L, Chen Q, Wan J, Yang GF (2006) Interactions of aryloxyphenoxypropionic acids with sensitive and resistant acetyl-coenzyme a carboxylase by homology modeling and molecular dynamic simulations. J Chem Inf Model 46:1819–1826
18. Zhu XL, Hao GF, Zhan CG, Yang GF (2009) Computational simulations of the interactions between acetyl-coenzyme-a carboxylase and clodinafop: resistance mechanism due to active and nonactive site mutations. J Chem Inf Model 49:1936–1943
19. Zhu XL, Yang WC, Yu NX, Yang SG, Yang GF (2011) Computational simulations of structural role of the active-site W374C mutation of acetyl-coenzyme-A carboxylase: multi-drug resistance mechanism. J Mol Model 17:495–503
20. Sali A, Blundell TL (1993) Comparative protein modelling by satisfaction of spatial restraints. J Mol Biol 234:779–815
21. Fiser A, Do RK, Sali A (2000) Modeling of loops in protein structures. Protein Sci 9:1753–1773
22. Marti-Renom MA, Stuart A, Fiser A, Melo F, Sali A (2000) Comparative protein structure modeling of genes and genomes. Ann Rev Biophys Biomol Struct 29:291–325
23. Laskowski RA, MacArthur MW, Moss DS, Thornton JM (1993) PROCHECK: a program to check the stereochemical quality of protein structures. J Appl Cryst 26:283–291
24. Vriend G, Sander C (1993) Quality control of protein models: Directional atomic contact analysis. J Appl Cryst 26:47–60
25. Eisenberg D, Lüthy R, Bowie JU (1997) VERIFY3D: assessment of protein models with three-dimensional profiles. Methods Enzym 277:396–404
26. Dauber-Osguthorpe P, Roberts VA, Osguthorpe DJ, Wolff J, Genest M, Hagler AT (1988) Structure and energetics of ligand binding to proteins: E. coli dihydrofolate reductase-trimethoprim, a drug-receptor system. Proteins Struct Funct Genet 4:31–47
27. Case DA, Darden TA, Cheatham TE, Darden T, Paesani F (2006) Amber 9. University of California, San Francisco
28. Duan Y, Wu C, Chowdhury S, Lee MC, Xiong G, Zhang W, Yang R, Cieplak P, Luo R, Lee T (2003) A point-charge force field for molecular mechanics simulations of proteins based on condensed-phase quantum mechanical calculations. J Comput Chem 24:1999–2012
29. Lee MC, Duan Y (2004) Distinguish protein decoys by using a scoring function based on a new Amber force field, short molecular dynamics simulations, and the generalized Born solvent model. Proteins 55:620–634
30. Wang J, Wolf RM, Caldwell JW, Kollamn PA, Case DA (2004) Development and testing of a general Amber force field. J Comput Chem 25:1157–1174
31. Jakalian A, Bush BL, Jack DB, Bayly CI (2000) Fast, efficient generation of high-quality atomic charges. AM1-BCC model: I. Method. J Comput Chem 21:132–146
32. Jakalian A, Jack DB, Bayly CI (2002) Fast, efficient generation of high-quality atomic charges. AM1-BCC model: II. Parameterization and Validation. J Comput Chem 23:1623–1641
33. Hawkins GD, Cramer CJ, Truhlar DG (1995) Pairwise solute descreening of solute charges from a dielectric medium. Chem Phys Lett 246:122–129
34. Hawkins GD, Cramer CJ, Truhlar DG (1996) Parametrized models of aqueous free energies of solvation based on pairwise descreening of solute atomic charges from a dielectric medium. J Phys Chem 100:19824–19839
35. Tsui V, Case DA (2001) Theory and applications of the generalized Born solvation model in macromolecular simulations. Biopolymers (Nucl Acid Sci) 56:275–291
36. Jorgensen WL, Chandrasekhar J, Madura J, Klein ML (1983) Comparison of simple potential functions for simulating liquid water. J Chem Phys 79:926–935
37. Darden T, York D, Pedersen L (1993) Particle mesh Ewald: an N log-(N) method for Ewald sums in large sysytem. J Chem Phys 98:10089–10092
38. Ryckaert JP, Ciccotti G, Berendsen HJC (1977) Numerical intergration of the Cartesian equations of motion of a system with constraints: molecular synamics of *n*-alkanes. J Comput Phys 23:327–341

39. Pastor RW, Brooks BR, Szabo A (1988) An analysis of the accuracy of Langevin and molecular dynamics algorithms. Mol Phys 65:1409–1419
40. Loncharich RJ, Brooks BR, Pastor RW (1992) Langevin dynamics of peptides: The frictional dependence of isomerization rates of N-actylananyl-N'-methylamide. Biopolymers 32:523–535
41. Berendsen HJC, Postma JPM, van Gunsteren WF, DiNola A, Haak JR (1984) Molecular dynamics with coupling to an external bath. J Comput Phys 81:3684–3690
42. Kollman PA, Massova I, Reyes C, Kuhn B, Huo S, Chong L, Lee M, Lee T, Duan Y, Wang W, Donini O, Cieplak P, Srinivasan J, Case DA, Cheatham TE (2000) Calculating structures and free energies of complex molecules: combining molecular mechanics and continuum models. Acc Chem Res 33:889–897
43. Wang JM, Morin P, Wang W, Kollman PA (2001) Use of MM-PBSA in reproducing the binding free energies to hiv-1 rt of tibo derivatives and predicting the binding mode to hiv-1 rt of efavirenz by docking and MM-PBSA. J Am Chem Soc 123:5521–5230
44. Huey R, Morris GM, Olson AJ, Goodsell DS (2007) A semiempirical free energy force field with charge-based desolvation. J Comput Chem 28:1145–1152
45. Turner JA, Pernich DJ (2002) Origin of enantiomeric selectivity in the aryloxyphenoxypropionic acid class of herbicidal acetyl coenzyme A carboxylase (ACCase) inhibitors. J Agric Food Chem 50:4554–4566
46. Délye C, Zhang XQ, Michel S, Matéjicek A, Powles SB (2005) Molecular bases for sensitivity to acetyl-coenzyme A carboxylase inhibitors in black-grass. Plant Physiol 137:794–806